IEEE Trans. Image Processing, 2014

Accurate Iris Recognition at a Distance Using Stabilized Iris Encoding and Zernike Moments Phase Features

Chun-Wei Tan, Ajay Kumar

Abstract:

Accurate iris recognition from the distantly acquired face or eye images requires development of effective strategies which can account for significant variations in the segmented iris image quality. Such variations can be highly correlated with the consistency of encoded iris features and the knowledge that such fragile bits can be exploited to improve matching accuracy. A non-linear approach to simultaneously account for both local consistency of iris bit and also the overall quality of the weight map is proposed. Our approach therefore more effectively penalizes the fragile bits while simultaneously rewarding more consistent bits. In order to achieve more stable characterization of local iris features, a Zernike moment-based phase encoding of iris features is proposed. Such Zernike moments-based phase features are computed from the partially overlapping regions to more effectively accommodate local pixel region variations in the normalized iris images. A joint strategy is adopted to simultaneously extract and combine both the global and localized iris features. The superiority of the proposed iris matching strategy is ascertained by providing comparison with several state-of-the-art iris matching algorithms on three publicly available databases: UBIRIS.v2, FRGC, CASIA.v4-distance. Our experimental results suggest that proposed strategy can achieve significant improvement in iris matching accuracy over those competing approaches in the literature, i.e., average improvement of 54.3%, 32.7% and *42.6% in equal error rates, respectively for UBIRIS.v2, FRGC, CASIA.v4-distance.*

1. Introduction

Iris recognition has emerged as one of the most promising technologies to provide reliable human identification. Remarkable iris recognition accuracy has been reported by the existing state-of-the-art iris recognition algorithms on the iris images acquired using near infrared (NIR) imaging from controlled environment [1]-[7]. Such superiority has made iris recognition as one of the most popular modalities for the very-large scale applications, such as in *Aadhar* project [8] to identify millions of citizens, or in border-crossing control system in UAE [45]. One major endeavor in the recent development of iris recognition technologies is to break through the

Copyright (c) 2014 IEEE. Personal use of this material is permitted. However, permission to use this material for any other purposes must be obtained from the IEEE by sending a request to pubs-permissions@ieee.org.

practicality limitations of the existing iris recognition systems to allow the image acquisition at-a-distance and under less controlled conditions [9]-[13]. Such properties are especially desirable in meeting the increasingly demand for forensic and high security surveillance applications [14]-[16]. Along with this initiative several iris databases composed of iris images acquired under less constrained environments have been released in public domain in order to encourage further research in this area. Among such databases, [12] and [13] are the attempts which employed visible illumination for image acquisition in order to overcome several limitations of the existing commercial iris recognition systems which are based on near-infrared (NIR) illumination. Currently popular NIR-based iris recognition approaches require high degree of active cooperation from the subjects to provide their eye images from close distance to the camera [1], [9], [10], which limit the applicability of the systems to be considered for forensic and surveillance applications.

The images acquired using visible imaging under less controlled environments are often noisier as compared to those acquired under NIR illumination and therefore require development of iris matching strategies which are more tolerant to noise. These images are usually influenced by multiple sources of noise, such as motion/defocus blur, occlusions from eyelashes, hair and eyeglasses, reflections, off-angle and partial eye images, as also shown from the sample eye images in Fig. 1. There have been some promising efforts devoted to develop more accurate iris segmentation approaches for such noisy eye images acquired using visible imaging [12], [14]-[23]. Further research in this emphasizes on developing robust feature extraction and matching algorithms which can accommodate inherent image variations in the segmented noisy iris images, for example, NICE.II competition [24]. Table 1 attempts to summarize the recent promising efforts on iris encoding and matching techniques from the iris biometrics literature. Apparently, none of the existing works have provided effective strategies for iris recognition acquired at-a-distance and under less constrained environments, using *both* the visible and NIR imaging.

(a) (b)

Fig. 1: Sample images acquired at-a-distance from less controlled environments using (a) visible imaging (b) NIR imaging.

Table 1: Recent prominent efforts on iris feature representation and matching techniques.

Ref.	Methodology	Employed Database, Operating Illumination And Number of Images/Subjects	Focused Problem	
			Verification (EER)	*Recognition (Rank-one)*
[28]	DCT-based encoding	• UBath$^{\wedge}$ – N/A images/150 subjects • CASIA$^{\wedge}$ – 2156 Images/308 subjects	Yes (2.59×10^{-4}, 5.55×10^{-4})	No (N/A)
[29]	2D DFT phase-based encoding	• CASIA.v1$^{\wedge}$ – 756 images/108 subjects • CASIA.v2$^{\wedge}$ – 1200 Images/60 subjects • ICE2005$^{\wedge}$ – 1425 images/124 subjects (right eye), 1528 images/120 subjects (left eye)	Yes (1.46×10^{-2}, 5.3×10^{-2} 3.3×10^{-2})	No (N/A)
[26]	Log-Gabor encoding with fragile bits estimation	• ICE2005$^{\wedge}$ – 1226 images/24 subjects (left eye)	Yes (N/A)	No (N/A)
[30]	Ordinal filter	• CASIA.v3$^{\wedge}$ – 2655 images/249 subjects • ICE2005$^{\wedge}$ – 1425 images/124 subjects (right eye), 1528 images/120 subjects (left eye) • UBath$^{\wedge}$ – 8000 images/200 subjects	Yes (2.28×10^{-3}, 3.48×10^{-3}, 4.39×10^{-4} 1.06×10^{-2}/5.72×10^{-3})	No (N/A)
[27]	Personalized weight map encoding	• CASIA.v3$^{\wedge}$ – 16212 images/411 subjects • ICE2005$^{\wedge}$ – N/A • UBath$^{\wedge}$ – 4000 images/400 subjects	Yes (0.8×10^{-2}, N/A, N/A)	No (N/A)
[31]	Log-Gabor encoding and recognition based on sparse representation.	• ICE2005$^{\wedge}$ – 1200 images/80 subjects (left eye) • ND-IRIS-0405$^{\wedge}$ – 1200 images/80 subjects • MBGC$^{\wedge}$ – 336 images/28 subjects	Yes (N/A)	No (N/A)
[37]	Log-Gabor encoding with periocular features	• UBIRIS.v2^{+} – 864 images/151 subjects (left eye) • FRGC^{+} – 500 images/150 subjects • CASIA.v4-distance$^{\wedge}$ – 935 images/131 subjects	Yes (N/A)	Yes (N/A)
This paper	Bits stabilization and localized ZMs phase-based encoding	• UBIRIS.v2^{+} – 864 images/151 subjects (left eye) • FRGC^{+} – 1085 images/149 subjects • CASIA.v4-distance$^{\wedge}$ – 935 images/131 subjects	Yes (2.90×10^{-2}, 1.196×10^{-1}, 1.986×10^{-1})	Yes (0.6304, 0.5575, 0.9496)

$^{\wedge}$ *NIR illumination* $^{+}$ *Visible illumination*

1.1 Motivation and Our Work

Iris recognition from distantly acquired eye images and under less constrained environments poses several challenges, especially for the images acquired using visible imaging. Image quality degradation is usually severer in the visible illumination eye images acquired from such dynamic environments. Most of the existing iris matching algorithms such as those in [7], [26]-[31] are developed for the NIR illumination eye images and may not perform robustly on the eye images acquired using visible illumination under less constrained conditions. Currently, there are very limited efforts in the literature that attempt to address limitations of popular iris matching algorithms on visible illumination images, with notable exceptions like those reported in [9], [25] from NICE.II competition. The winning algorithm from this competition is largely attributed to the use of multimodal strategy by employing multiple pieces of information from iris, periocular, color distribution, *etc*. to further improve the recognition accuracy [32]. Therefore, such performance improvement is quite intuitive/expected and can be largely attributed to the multi-biometrics strategy, rather than any effort that solely considers the iris information.

Our key motivation in this work has been to develop a more robust and accurate iris encoding and matching strategy which can be effective for both *NIR* and *visible* illumination eye images acquired *remotely* and under less constrained environments. The development of iris recognition technologies capable of operating under less-constrained imaging environment requires that imaging constraints on the illumination requirements should be relaxed. Therefore the need is to develop robust iris recognition algorithms that can simultaneously operate on iris images acquired under visible or near infrared illumination. The iris encoding and matching strategy developed in this work consists of a global iris bits stabilization encoding stage and a localized Zernike moments phase-based encoding stage. Such complementary matching information can be simultaneously acquired from both global and localized encoding strategies and is expected to provide more accurate iris recognition capability (see Section 5). The global iris encoding strategy has its strength in less noisy iris region pixels, while the localized iris encoding strategy can be more tolerant to imaging variations and noise. The global encoding strategy exploits the knowledge of fragile (inconsistent) bits from a set of partially overlapping normalized iris images. The consistency of each of the iris bit is indicated by a probability value such that a more consistent bit is represented with higher value while an inconsistent bit is represented with the lower value. A non-linear approach is proposed in this paper which can more effectively penalize the fragile bits while simultaneously reward the more consistent iris bits. Such non-linear approach not only considers the consistency of each iris bit, but takes into the account the overall quality of the estimated probability map. In order to achieve a more stable characterization of local iris features from noisy iris region pixels, we propose a new strategy to encode and match local iris features using phase encoding of Zernike moments (ZMs). The ZMs have been shown to constitute robust image features which are more tolerant to noise, information redundancy, viewpoint change, partial occlusion, *etc*. [33]-[36]. Such properties are highly desirable in order to accommodate for noise and imaging quality variations as commonly observed in the visible illumination eye images acquired under less constrained environments. Unlike ref. [47], the key novelty of the proposed ZMs phase-based encoding strategy lies in recovering discriminative features from the localized iris region pixels. Such localized encoding strategy has shown to be effective to better accommodate for noise and image variations in localized iris region pixels. Furthermore, the computation of ZMs features over the localized regions can offer more computational efficiency as it only involves computation of low order of

moments (see Table 3). The influence from the occlusion noise (e.g. eyelids, eyelashes and reflection) is crucial and should be mitigated from deteriorating the recognition performance [2], [3]. As such, a parameter γ is introduced to weight the ZMs phase-based features in order to mitigate the possible influence from the identified occluded iris pixels. Such parameter is computed from the occlusion mask automatically obtained during the iris segmentation phase. We employ only the ZMs phase[*] component as it has been shown to provide more discriminative power than the magnitude component [36]. The similarity of any two ZMs phase-based encoding features can be obtained by computing the cross-phase distance. The proposed approach is evaluated on subsets of images from three publicly available databases: UBIRIS.v2, FRGC and CASIA.v4-distance, which suggests significant improvement than several competing iris matching approaches, as the average improvements of *54.3%*, *32.7%* and *42.6%* in Equal Error Rates are respectively achieved on the three employed databases. The main contributions of this paper can be summarized as follows:

- Iris images acquired under less constrained imaging environments are most likely to be influenced by variations from multiple sources. Therefore, this paper proposes a new approach to robustly encode iris features using phase information of the Zernike moments (see Section 4.2).
- A global iris bits stabilization encoding strategy is proposed (see Section 4.1). A nonlinear approach is introduced to more severely penalize iris bits for their fragility while simultaneously rewarding others for their consistency. The consistency of such iris bits is automatically estimated based on the knowledge of fragile bits.
- We develop a joint strategy to more accurately match iris images, especially those acquired *at-a-distance* and under *less constrained* environment, by simultaneously exploiting the local and global iris features. The global iris encoding strategy has its strength in less noisy iris region pixels, while the localized iris encoding strategy can be more tolerant to image variations and noise The supplementary matching information acquired from both the global and localized iris features has been shown to achieve more accurate recognition accuracy, as estimated from the experiments on three publicly

[*] Most commercial iris recognition systems are based on iris codes [2] which only use phase information rather than the magnitude information.

available databases, as compared to several competing approaches from the literature (see Section 5).

The remainder of this paper is organized as follows. In Section 2, we provide review on some related works reported from the literature. In section 3, we briefly describe the iris segmentation step for automatically extracting iris region. In Section 4, the proposed global iris bits stabilization encoding and localized ZMs phase-based encoding are detailed. In Section 5, we provide the performance evaluation on the proposed iris encoding and matching strategy, as well as the comparison with other competing iris matching approaches from the literature. Lastly, discussion and conclusion from this paper are respectively presented in Section 6 and 7.

2. Related Work

Almost all the existing commercial iris recognition systems employ a matching model which is based on the binarized iris codes. Such iris codes are generated from the phase quantization of the filter responses, for *e.g*. *Gabor* filter [1]-[3]. Reference [26] presented the first comprehensive work in the literature which recovered the existence of fragile bits in the widely employed iris code. These fragile bits usually occur near the axes on the complex plane, which may be attributed to the segmentation error, alignment issues, and choice of the employed filter. Fragile bits are regarded as iris bits which are temporally inconsistent, *i.e*. the values of some bits are flipping between 0 and 1 across the iris codes of the same subject which are acquired at different time instance. Fragile bits are learned from the iris codes of each registered subject in the system and therefore considered to be personalized to each subject enrolled in the system. In order to determine the fragile bits, a global threshold τ must be predetermined. Let θ_n denote the number of times that *n*-th bit is fragile estimated from the K iris codes of same subject. The *n*-th bit is considered to be fragile if $\theta_n/K \geq \tau$. However, the use of the global threshold τ may not be adequate since different levels of the fragility can be expected to occur in the iris codes of each distinct subject. The approach described in [27] can be considered as a further research effort in overcoming such limitation by employing a personalized weight map iris matching strategy. Instead of using a global threshold, each *n*-th bit is weighted based on its consistency by using a normalized nonlinear compressive function, as defined as: $w_n = 2\frac{{\theta_n}^2 - (K-\theta_n)^2}{K^2} - 1$.

3. Iris Segmentation

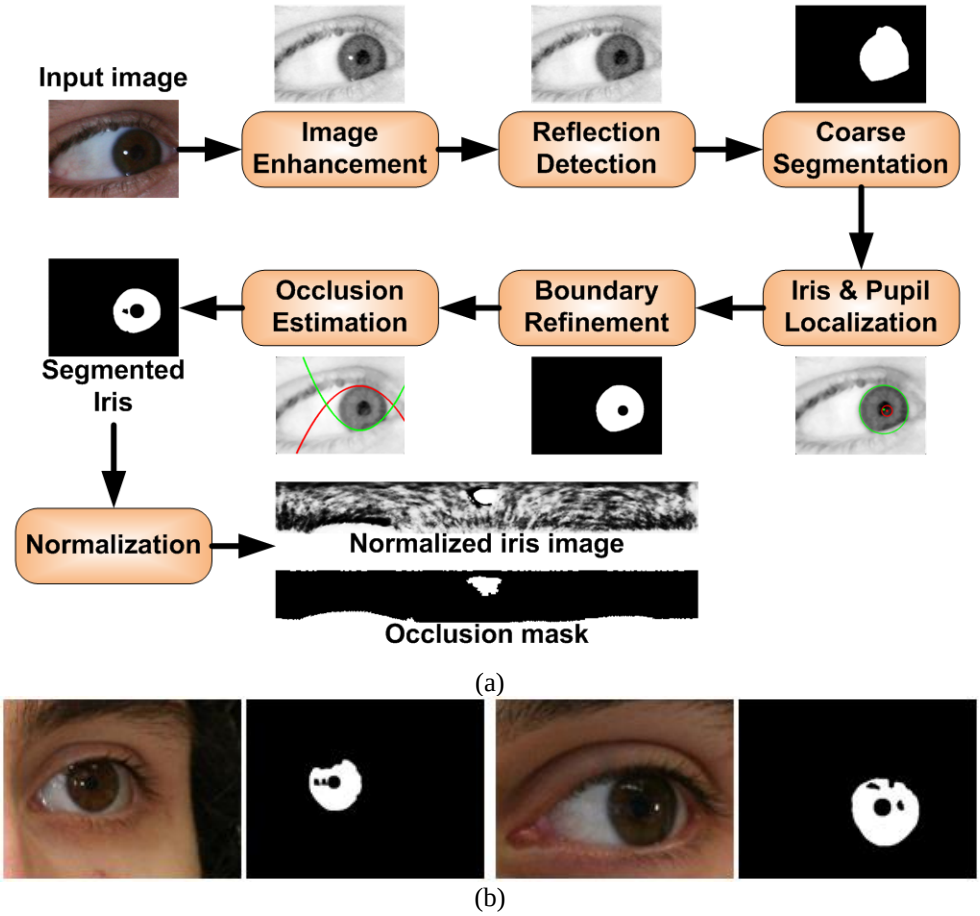

Fig. 2: Iris segmentation. (a) Block diagram to show various steps involved in iris segmentation. (b) Sample segmentation results from UBIRIS.v2 database (image ID: C484_S1_I5 and C516_S1_I11).

Efficient and robust iris segmentation algorithm is crucial for any successful iris recognition strategy in order to automatically extract iris region from the eye image. Fig. 2(a) shows the major iris segmentation steps employed in this paper to automatically localize the iris region. The iris segmentation process starts with the image enhancement that uses retinex algorithm in order to improve the contrast between limbic and pupillary boundaries. A low pass filter is applied to suppress the high frequency contents in the enhanced image. Such attenuation step is important and helps to improve the robustness of the segmentation. Source reflection is another commonly observed source of noise in the acquired eye images and can be attributed to the ambient illumination. The reflection detection step aims to detect image pixels influenced by the reflection noise. The detected noisy pixels are filled and a binary mask which indicates all such noisy pixels is generated. Thereafter a random walker based algorithm is employed to perform coarse segmentation of iris region. The localization of limbic and pupillary boundaries is then

approximated from the coarsely segmented iris region based on circular model. The boundary refinement step is responsible to further refine the approximated limbic and pupillary boundaries. The last step of the iris segmentation involves estimation of occlusion noise such as eyelashes, shadow and eyelids. The identified occluded and reflection pixels are masked in order to be excluded during the iris matching stage. Fig. 2(b) shows two sample segmentation results from the UBIRIS.v2 database. In order to account for the varying iris size due to the imaging distance between the eye and the acquisition device, as well as the pupillary response to ambient light which results in dilation or constriction of the pupil, Daugman's rubber sheet model is employed to normalize the segmented iris image by performing a mapping from the Cartesian coordinates to the doubly-dimensionless polar coordinates [2]. More details on the employed iris segmentation algorithm can be obtained from reference [37].

4. Proposed Feature Encoding and Matching Strategy

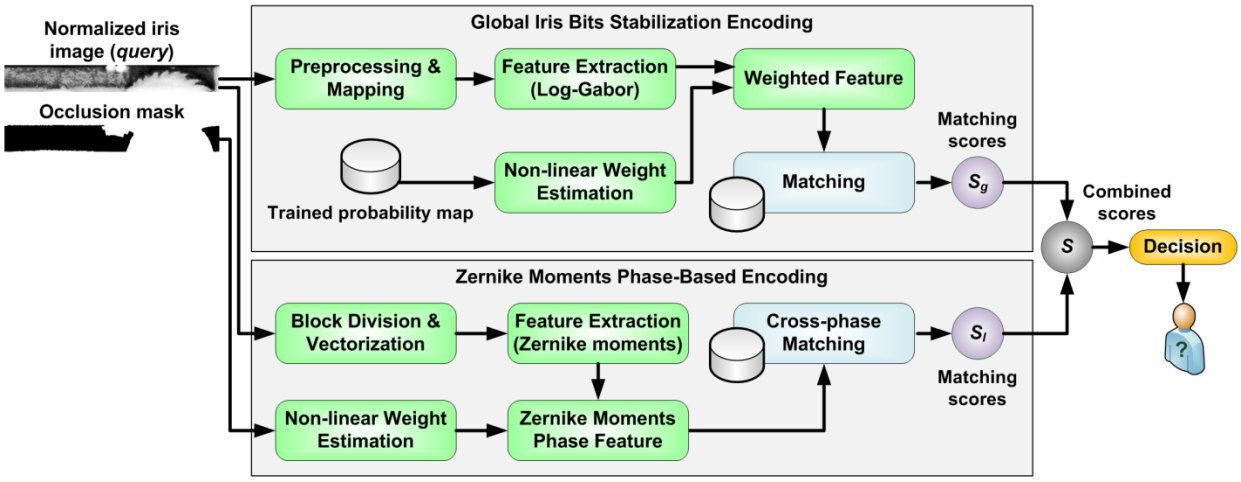

Fig. 3: Block diagram of the proposed joint iris recognition strategy using global and localized iris features encoding.

The block diagram of the proposed iris matching strategy based on the global iris bits stabilization encoding strategy (Section 4.1) [45] and a localized ZMs phase-based encoding strategy (Section 4.2) is shown in Fig. 3. The global iris bits stabilization encoding strategy is motivated from the recent promising approaches in [26], [27], and exploits the weight maps in such manner that higher (lower) weights are assigned to the quantized iris bits which appear to be stable/consistent (fragile). Such weighting strategy is observed to be more effectively in emphasizing (penalizing) the high (low) discriminative iris features, especially for the noisy iris images acquired under less constrained environments. As such, a non-linear weighting strategy

based on power law is proposed to adaptively weight the extracted global iris features. In spite of having better discriminative power over the conventional approaches [2]-[3], [7], [29], [30], [37], the global iris encoding strategy is still not adequate to accurately characterize the iris features extracted from the distantly acquired eye images under less constrained environments, which are generally have higher variations (e.g. scale change, illumination change, defocus and translation). In order to achieve a more stable characterization of local iris features, we propose a new iris extraction scheme using phase encoding information of the ZMs. The ZMs have been shown to constitute robust image features which are less sensitive to noise, information redundancy, viewpoint change, partial occlusion, *etc*. [33]-[36], and therefore can be used as a powerful descriptor to account for such variations in distantly acquired eye images. The localized ZMs features are computed from the partially overlapping image blocks extracted from the normalized iris image. The advantages of employing such localized phase-based encoding strategy are two folds. Firstly, the local pixel variations can be better recovered from the localized iris region. Such localized phase-based encoding strategy can be more tolerant to feature distortion (due to nature of features) in local region pixels, and therefore can be exploited to complement the global encoding strategy in order to achieve more accurate recognition accuracy. Secondly, the phase encoding information of the ZMs has shown to offer more discriminative power than the magnitude information in local region pixels, as also in [36]. In order to mitigate the effect from the identified occluded iris pixels, a parameter γ is introduced to weight the computed ZMs features. This parameter γ is estimated from the occlusion mask which is automatically obtained during the iris segmentation stage. A joint strategy is employed to simultaneously combine both the extracted global and localized iris features. Such combined information can allow us to make better decisions and benefit from the outcome of matching performance using local texture matches which are more tolerant to variations/noise, and also the global iris texture matches which have its strength in less noisy iris region pixels.

4.1. Global Iris Feature Representation

A. Preprocessing for Normalized Iris Images

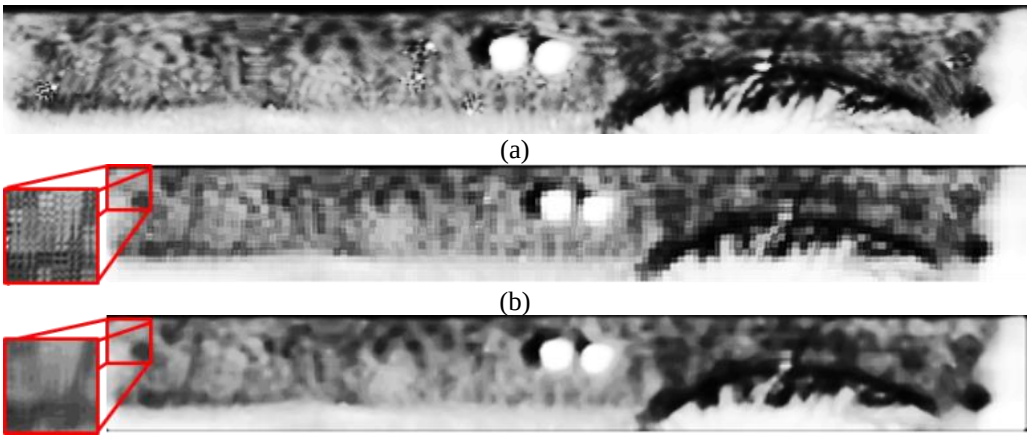

Fig. 4: Overlapping block strategy. (a) Normalized iris image (ID: S4011D00), (b) Remapped normalized iris image, (c) smoothen of (b). (Note that the actual image size of (b) and (c) are larger than the (a), and therefore they are resized to better utilization of space).

The accuracy of the iris segmentation and the effectiveness of the feature encoding are the essential core for any successfully iris recognition application. Most of the commonly observed noise sources such as occlusions from eyelashes, eyelid, hair, eyeglasses and specular reflections in the eye images can be usually identified and masked during the iris segmentation process. However, the eye images acquired at-a-distance and under less constrained environments are tend to be noisier not only due to the influences from the commonly observed noise sources but also from the imaging quality variations. Such phenomenon is even more noticeable from the eye images acquired using visible illumination imaging. In order to mitigate such influences, preprocessing is firstly applied to the normalized iris images by employing an overlapping block strategy, as given as follows:

$$f_{b,s}: \mathbb{R}^2 \rightarrow \mathbb{R}^2 \tag{1}$$

where f is a function to extract the image blocks of size $b \times b$ from the normalized iris image I, sliding at an interval of s pixels in both the horizontal and vertical directions. The interval s is defined as half of the block size, *i.e.* $s = b/2$ for all the employed databases in this paper. The remapped normalized iris images contain blocking artifacts as a result of the overlapping block operation. Such blocking artifacts are undesired as may introduce spurious frequency content during the iris feature extraction stage. In order to alleviate the effect from the blocking artifacts, a two-dimensional median filter of size $b \times b$ is applied to the remapped normalized iris images,

as illustrated in Fig. 4. The employed overlapping block strategy is observed to achieve improved recognition performance. There are two possible reasons to justify the advantages of the overlapping block strategy. Firstly, the information redundancy is achieved across the neighboring image blocks. Such redundant information can be exploited to better account for spatial variations in the normalized iris images, especially for those acquired under less constrained environments. Secondly, the smoothing operation by employing the median filter not only mitigates the effect from the blocking artifacts but also simultaneously suppresses the noise in each image block.

B. Iris Bits Stabilization

The existence of the fragile bits has been observed and effectively used in [26] to improve the matching accuracy. Reference [27] further extended this work based on the knowledge of fragile bits by weighting each bit to achieve improved recognition performance. The eye images acquired under less constrained environments are often degraded by noise, and the observation shows that the occurrence of noise is even more evident in the eye images acquired under visible illumination [14], [16], [32]. Therefore, the previous strategies as in [26]-[27] can be further exploited to work on the noisy eye images which are acquired under less constrained environments. The fragile bits which are estimated from the training images can be considered as an outcome from the noise perturbation.

As such, we propose a nonlinear weighting strategy to quantify the consistency of each iris bit in the remapped normalized iris image. The iris bit which is more consistent will be assigned with higher weight (close to one) to emphasize its importance while the iris bit which is less consistent is assigned with a lower weight (close to zero). Given *K* preprocessed training normalized iris images $\{\hat{I}_i^j\}_{i=1}^K$ of *j*-th class, we first obtain the corresponding iris code representations $\boldsymbol{C}^j = \{C_i^j\}_{i=1}^K$. Next, the consistency of *n*-th bit can be estimated from the $\boldsymbol{C}^j$ by measuring the number of times that the *n*-th is fragile. Note that the $\boldsymbol{C}^j$ is aligned with respect to the minimum Hamming distance obtained from the circular bit shifting before the consistency of iris bits is estimated. Let θ_n denote the number of times that *n*-th bit is fragile. Then the consistency of *n*-th bit can be indicated based on a probability value, as defined as follows:

$$p_n^j = 1 - \frac{\theta_n}{K} \in [0, 1] \tag{2}$$

Hence, a probability map $P^j = \{p_1^j, p_2^j, \dots, p_N^j\}$ can be obtained based on the knowledge of the fragile bits estimated from some iris codes $\boldsymbol{C}^j$. The P^j has the identical dimension as the iris code of *N* bits, with each p_n^j corresponding to the consistency of the *n*-th iris bit. Fig. 5 shows two examples of the probability maps obtained from the five iris codes. It can be observed that the iris bits where are estimated to be more consistent have higher probability values (higher intensity values), while the iris bits which are less consistent are indicated by lower probability values (lower intensity values).

In order to more effectively emphasize (penalize) those bits which are highly consistent (inconsistent), a non-linear weighting strategy is introduced as follows:

$$w_n^j = \left(p_n^j\right)^{\alpha^j} \tag{3}$$

$$\alpha^j = \begin{cases} \dfrac{|P_{max}|}{\mu^j} = \dfrac{1}{\mu^j} & \text{if } \mu^j > 0 \\ 1 & \text{if } \mu^j = 0, \end{cases}$$

where $\mu^j = {}^1\!/_N \sum_{n=1}^{N} p_n^j$; P_{max} indicates the maximum probability value of *P*. The α^j takes the similar form as crest factor (peak-to-average ratio) which is employed to indicate the overall quality of the P^j. The weighting function in Eq. (3) exhibits several interesting properties which can be summarized as follows:

- The weighting function *preserves* the local consistency value for the highly consistent (inconsistent) bits, *i.e.* when $p_n^j = \{0,1\}$, regardless of the crest factor α^j. As such, the weights for those highly consistent (inconsistent) bits will not be affected by α^j.
- For $\mu^j = \{0, 1\}$, which are the two special cases when the crest factor at its extremum, the weight remains the same, *i.e.* $w_n^j = p_n^j$.
- For $K = 1$, the computed weight map $W^j = \{w_1^j, w_2^j, \dots, w_N^j\}$ is identical to the generated iris code C^j , such that the $w_n^j = \{0,1\}$. Therefore, the Eq. (3) can be considered as the generalized representation for the conventional iris code representation.

The similarity between a query iris code C_{query} and reference gallery iris code $C_{gallery}^j$ of class *j* can be computed using modified Hamming distance as given as follows [27]:

$$HD^j = \frac{\left\|\left(C_{query} \oplus C_{gallery}^j\right) \times W^j\right\|}{\|W^j\|} \tag{4}$$

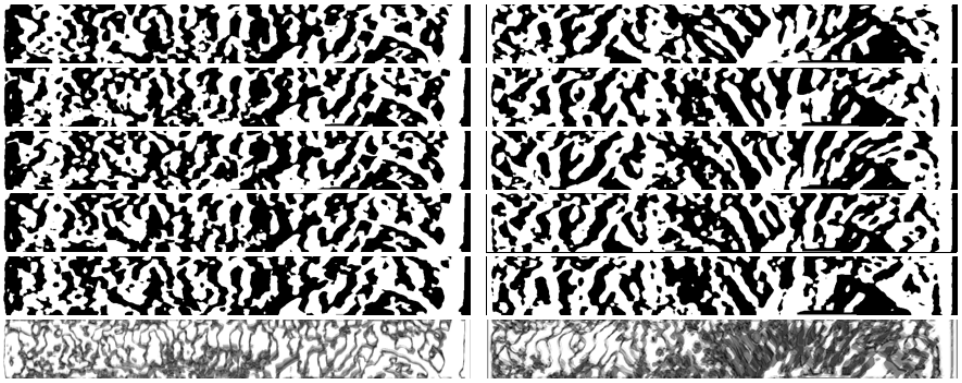

Fig. 5: Examples of the probability map (last row) estimated from five iris codes (first five rows) from CASIA.v4-distance database (Image IDs: {S4011D00, S4011D01, S4011D02, S4011D03, S4011D04}, {S4023D00, S4023D01, S4023D02, S4023D03, S4023D04}). Brighter pixel indicates the bit is more stable while darker pixel indicates otherwise.

4.2. Zernike Moments Phase-based Encoding

Zernike moments are well known to recover scale, rotation and translation invariance features and have been employed in many image processing applications, including in iris segmentation [15]-[16], image reconstruction [34]-[35], *etc*. However, prior attempts *only* exploited the magnitude information of the ZMs in order to benefit from the rotation invariance property. The coarse *phase* information (iris code) as detailed in [2]-[3] has been successfully employed to characterize the iris texture. Such an approach for iris matching has shown to achieve accurate iris matching for large-scale iris recognition applications but under constrained and NIR-based image acquisition. However, image variations such as scale changes, illumination changes, geometric transformation, *etc*., are often embedded in the eye images acquired at-a-distance and under the less constrained environments, which further increase the difficulty in performing the iris encoding and matching for such noisy iris images. Therefore we propose a new iris encoding and matching strategy by exploiting the *phase* information of the ZMs extracted from the partially overlapping local iris region pixels. The motivations for using ZMs *phase*-only information to encode such localized iris texture information are as follows: (1) The *phase* information has been demonstrated to provide better discriminative power than the magnitude information, while retaining the scale invariant properties of the ZMs to accommodate inherent image variations from less constrained imaging [36]; (2) the local pixel variations can be better recovered from the localized iris region rather than those accumulated globally from the phase difference in conventional iris encoding. Such *phase* encoding information of the ZMs from the local region pixels is expected to be more tolerant to the feature

distortions than the global encoding scheme, and therefore can be used to complement the global iris features matching for achieving more accurate performance.

A. Zernike Moments

The Zernike moments with order β and repetition α constitute a set of orthogonal basis functions $\{V_{\beta\alpha}(\rho,\tilde{\theta})\}$ which are defined over a unit circle in the polar coordinates as follows [34], [36]:

$$V_{\beta\alpha}(\rho,\tilde{\theta}) = R_{\beta\alpha}(\rho)e^{j\alpha\tilde{\theta}} \tag{5}$$

$$R_{\beta\alpha}(\rho) = \sum_{k=0}^{p}(-1)^k \frac{(\beta-k)!}{k!\,(p-k)!\,(q-k)!}\rho^{\beta-2k}$$

where $p = (\beta - |\alpha|)/2$ and $q = (\beta + |\alpha|)/2$; β is a non-negative integer and α is an integer that satisfies the conditions: $|\alpha| \leq \beta$ and $\beta - |\alpha| =$ even. ZMs for an image function $I(\rho,\tilde{\theta})$ can be obtained by projecting the $I(\rho,\tilde{\theta})$ onto $\{V_{\beta\alpha}(\rho,\tilde{\theta})\}$, as represented by:

$$Z_{\beta\alpha} = \frac{\beta+1}{\pi}\int_0^{2\pi}\int_0^1 I(\rho,\tilde{\theta})V^*_{\beta\alpha}(\rho,\tilde{\theta})\,\rho\;d\rho\,d\tilde{\theta} \tag{6}$$

where $V^*_{\beta\alpha}$ denotes the complex conjugate of Eq. (5).

B. Localized Iris Representation

The localized ZMs features are computed from the image blocks B of size $\tilde{b}\times\tilde{b}$ extracted from the normalized iris image I, sliding at an interval of $\tilde{s}$ pixels in both the horizontal and vertical directions. The interval $\tilde{s}$ is defined as half of the block size, *i.e.* $\tilde{s} = \tilde{b}/2$ for all the employed databases in this paper. Let N_B denote the total number of extracted image blocks $\{B_i\}_{i=1}^{N_B}$. The ZMs from order one up to order β at repetition α are computed for each B_i, which form a feature vector $\boldsymbol{Z}$ as represented as follows:

$$\boldsymbol{Z} = \gamma\left[Z^1_{1\alpha}, Z^1_{2\alpha}, \dots, Z^1_{\beta\alpha}|\dots|Z^{N_B}_{1\alpha}, Z^{N_B}_{2\alpha}, \dots, Z^{N_B}_{\beta\alpha}\right]^T \tag{7}$$

The parameter $\gamma \in [0,1]$ is introduced in Eq. (8) which serves to mitigate the effect of the occlusion noise to the computed ZMs features. Such γ is defined and can be computed as follows:

$$\gamma = \frac{2\xi}{1+\xi^2} \tag{8}$$

$$\xi = 1 - \frac{O_{noise}}{W\times H}$$

where O_{noise} denotes the total number of occluded iris pixels (white) which are identified from the automatically extracted $W \times H$ occlusion mask during the iris segmentation process.

In order to measure the similarity s between two given feature vectors $\boldsymbol{Z}_{query}$ and $\boldsymbol{Z}^{j}_{gallery}$ of class j, we employ a phase distance function which is defined as follows:

$$s^{j} = \left\| \varphi\left(\frac{\boldsymbol{Z}_{query} \circ \boldsymbol{Z}^{*j}_{gallery}}{\left| \boldsymbol{Z}_{query} \circ \boldsymbol{Z}^{*j}_{gallery} \right|} \right) \right\|_2 = \| \varphi(R) \|_2 \tag{9}$$

$$\varphi(R) = \arctan\left(\frac{\mathrm{Imag}(R)}{\mathrm{Real}(R)} \right)$$

where $\mathrm{Real}(.)$ and $\mathrm{Imag}(.)$ respectively denote the real and imaginary parts of R; '$\circ$' denotes the entry-wise product; '$*$' denotes the complex conjugate. Higher similarity between phase angles of the ZMs will result in lower values of S (close to zero) while higher dissimilarity will result in higher values. It can be observed that the phase information computed from the iris images of the same subject, for example in Fig. 6(a) and (b), are highly correlated.

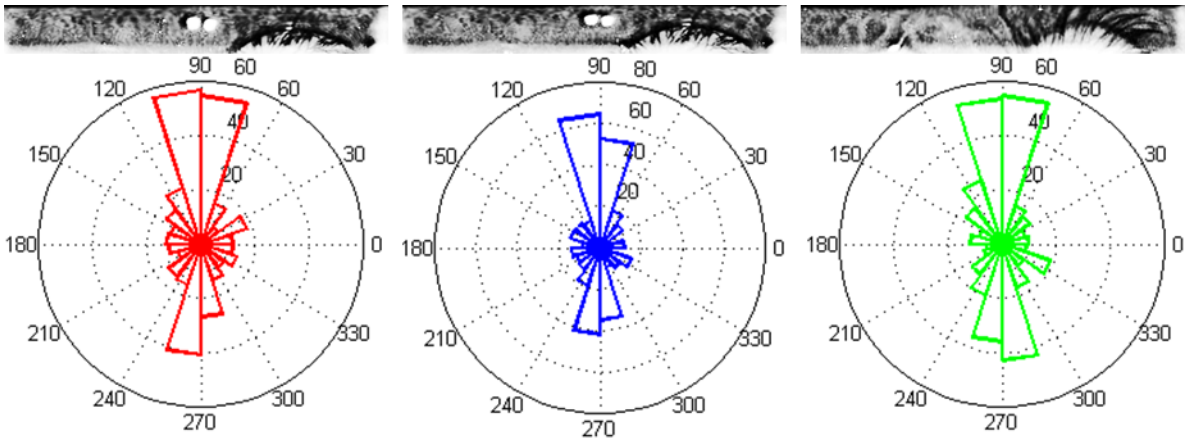

(a) (b) (c)

Fig. 6: Phase angle information for three Zernike features respectively computed from the normalized iris images from CASIA.v4-distance database with ID: (a) S4011D00, (b) S4011D01, (c) S4023D01. Features (a) and (b) are computed from the images of the same class. The varying angles represent the encoded iris features using the phase information of the ZMs. The similarity scores between (a) and (a), (a) and (b), and (a) and (c) are $\boldsymbol{s(a,a) = 0}$, $\boldsymbol{s(a,b) = 16.624}$ and $\boldsymbol{s(a,c) = 27.218}$, respectively.

5. Experiments and Results

In this section, we detail on the experiments and present the experimental results obtained from the three publicly available databases: UBIRIS.v2 [24], [13], FRGC [38], [39], and CASIA.v4-distance [40] to ascertain the performance from the proposed iris encoding and matching strategy.

The three employed databases were *distantly* acquired (ranging from 3-8 meters) under less constrained environments using either *visible* or *NIR* imaging, and therefore appropriate for the research problem focused in this paper. All the eye images employed in this paper use automated iris segmentation approach described in [37], which has shown to be more accurate as it achieves superior segmentation accuracy for both the iris images acquired under visible and NIR illumination.

5.1. Databases and Parameters Selection

Table 2: Numbers of images and subjects of the employed databases

Database	**UBIRIS.v2**	**FRGC**	**CASIA.v4-distance**
Imaging type	Visible	Visible	NIR
Number of images	864	1085	935
Number of subjects	151	149	131

Table 3: Parameters employed by the proposed approach

Parameter / **Database**	***Global Feature***		***Localized ZMs Feature***		
	Wavelength	**SigmaOnf**	**Block Size**	$\boldsymbol{\beta}$	$\boldsymbol{\alpha}$
UBIRIS.v2	59	0.32	25	1	1
FRGC	40	0.35	17	1	1
CASIA.v4-distance	20	0.25	25	3	1

All the experiments performed in this work use subsets of images from the three employed databases, as summarized in the Table 2. The segmented iris images from UBIRIS.v2, FRGC, and CASIA.v4-distance databases are respectively normalized to the sizes of 512×64, 256×32 and 512×64. The global iris features are extracted by employing 1D log-Gabor filter [7], [41], and the parameters *wavelength* and *SigmanOnf* for the three employed databases are given in Table 3. These parameters are obtained from a set of training images which are independent from the test images in the respective databases. These parameters essentially represent the best combinations, as computed during the training phase, to minimize the equal error rate achieved from matching all the images in the training dataset. For CASIA.v4-distance database, the images from the first 10 subjects are employed to train the log-Gabor parameters, while the first eight left eye images from the rest of the 131 subjects are employed for testing or performance evaluation. For UBIRIS.v2 database, a subset of 1000 images from 171 subjects as released in [24] is employed in the experiments. The 96 images from the first 19 subjects are employed for

selecting (training) the log-Gabor parameters[†] while the rest of the segmented eye images are employed as independent test images for the performance evaluation. Similarly, a subset of high-resolution still images from the FRGC database is employed in the experiments. The eye images are selected from sessions 2002-269 to 2002-317 of Fall2002 and Spring2003 by using an open source eye detector [48], and the selected eye images comprise a total of 1085 images from 149 subjects. For the color images, we employ the luma-channel (Y) of the YCbCr after the color space conversion from the RGB color space. As for the performance evaluation, we further divide the remaining images into gallery dataset and test dataset. The gallery dataset is employed for estimation of probability maps as detailed in Section 4.1. In addition, subsets of the images from the gallery dataset of the employed databases are randomly chosen in order to determine the parameters (see Table 2) for the localized ZMs phase-based encoding scheme as detailed in Section 4.2. In this paper, we employ at most[‡] (first) *five* images as the gallery dataset while the remaining images as the test dataset for the performance evaluation.

5.2. Combination of Global and Local Matching Scores

In order to simultaneously employ the matching information computed from both global and localized iris encoding schemes, the approaches presented in Sections 4.1 and 4.2 are combined at score level using weighted sum rule, *i.e.* $score = w_1 \times score_1 + w_2 \times score_2$ and $w_1 + w_2 = 1$. The receiver operating characteristic (ROC) and cumulative match characteristic (CMC) computed using the three employed databases are shown in Fig. 7 and Fig. 8 respectively. It can be observed that the recognition performance from the *phase* encoding using ZMs clearly outperforms those using the magnitude encoding using (same) ZMs on all the three employed databases. These results further verify the argument that the *phase* information of ZMs can offer significantly higher discriminative power than the magnitude information. Furthermore, the significantly improved performance achieved from our experimental results suggests superiority of the proposed joint matching scheme by simultaneous using the global and localized iris features. The combined scores from the global and localized iris features can offer better discrimination capability than those employing either global or localized iris representation alone.

[†] We used the same protocol as in previous work in [16] and [37].
[‡] The number of images is varying for each distinct subject for UBIRIS.v2 and FRGC databases as some poor segmented/quality images were filtered out by the completely automated segmentation algorithm [37].

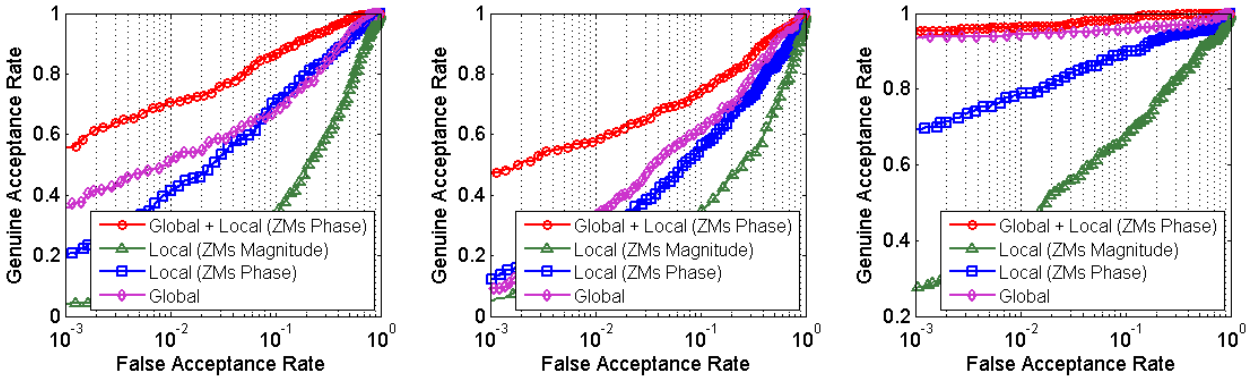

(a) (b) (c)

Fig. 7: Receiver operating characteristics from the proposed approach on (a) UBIRIS.v2, (b) FRGC, (c) CASIA.v4-distance database.

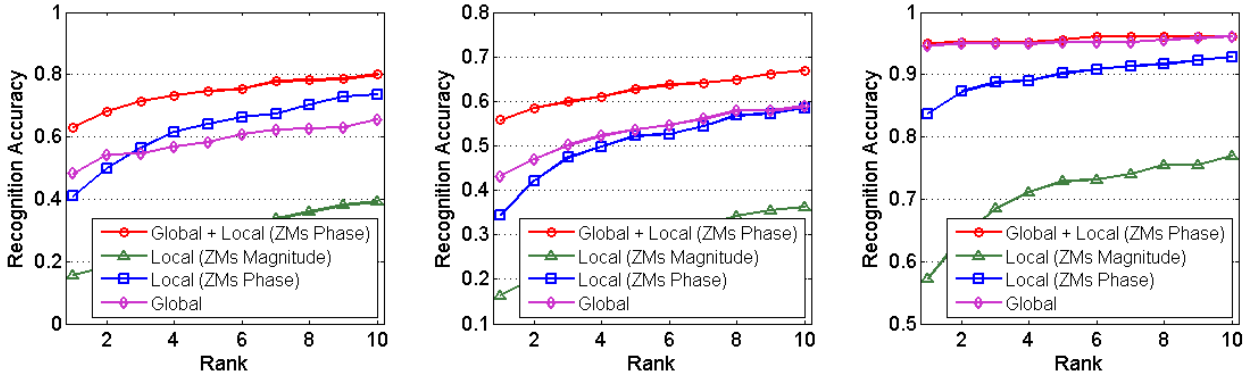

(a) (b) (c)

Fig. 8: Cumulative match curves from the proposed approach on (a) UBIRIS.v2, (b) FRGC, (c) CASIA.v4-distance database.

5.3. Performance Comparison

We also performed comparison with several competing iris matching approaches presented in the literature: Fragile Bits [26], Personalized weight map (PWMap) [27], band-limited phase only correlation (BLPOC) [29], log-Gabor [37] and Sparse [31][§]. The ROC and CMC curves obtained from the various approaches evaluated under the *same* protocol are respectively shown in Fig. 9 and Fig. 10. The equal error rate (EER) and the decidability index (*d*') are two most common performance indexes employed in the iris biometrics in the literature [25], [27], [30], [32]. The estimated recognition performance from the various iris matching approaches in this work as indicated using EER and *d*' are summarized in the Table 4. These results suggest that the proposed iris matching strategy outperforms other competing approaches with both the achieved EER and the decidability index. The achieved EER and *d*' have been respectively improved from

[§] The source code is publicly available at:
http://www.umiacs.umd.edu/~jsp/Research/SRRecognition/SparseRecognitionCancelability_PAMI2010.zip

0.1922 to 0.1196 and 1.5843 to 2.5735, as compared to best of the reported methods (*i.e.* Sparse [31]) from the experiment on UBIRIS.v2 database. For the experiment on FRGC, the EER and *d*' are respectively improved from 0.2397 to 0.1986 and 1.4298 to 1.8899, as compared to the best of reported method in [31]. For the experiments on CASIA.v4-distance database, the EER is improved from 0.0385 to 0.0290, as compared to the approach [37], while the *d*' is improved from 3.4345 to 6.4735, as compared to the approach [31]. Fig. 12 illustrates the percentages of improvement for the proposed approach in terms of EER as compared to the other methods. In summary, the proposed iris matching approach achieves significant improvement over several state-of-the-art iris matching algorithms, which suggests average percentage of improvement of *54.3%, 32.7%* and *42.6%* respectively on UBIRIS.v2, FRGC and CASIA.v4-distance databases. In order to establish a fairer comparison, we made another attempt to compare the proposed strategy with the combination of the best two methods reported from each of the employed databases. The matching information from the two methods are combined at score level based on the weighted sum rule, and the parameter employed for such fusion is summarized in Table 5. As illustrated in Fig. 11, the proposed strategy again outperforms the joint strategy from the best two reported methods from our experiments, which further confirm the effectiveness of proposed joint global and localized iris recognition. The effectiveness of the proposed joint matching strategy can be largely attributed to the use of complementary matching information from both the global and localized iris region pixels. As discussed earlier, the localized iris encoding strategy is expected to be more tolerant to the inherent at-a-distance imaging variations and noise, while the global iris encoding strategy has its strength in accurate matching of least noisy iris region pixels; as such observation is also reflected from the fusion weights as employed for the joint matching strategy. It can be noted that the challenging visible illumination eye/face databases, *i.e.*, UBIRIS.v2 and FRGC, higher weights are assigned for the localized encoding method. For the CASIA.v4-distance database in which better quality of the eye images have been acquired, higher weight is assigned to the global encoding method. Therefore, it is reasonable to argue that the complementary matching information from the joint global and localized iris encoding scheme can provide higher accuracy in recognizing the iris images acquired at-a-distance and under less constrained environments.

Table 4: The equal error rates and decidability indexes reported from various iris matching approaches

	UBIRIS.v2		FRGC		CASIA.v4-distance	
Method	**Equal Error Rate**	**Decidability Index**	**Equal Error Rate**	**Decidability Index**	**Equal Error Rate**	**Decidability Index**
Sparse [31]	0.1922	1.5842	0.2397	1.4298	0.0445	3.4345
PWMap [27]	0.2608	1.37	0.2681	1.1448	0.0564	3.4170
Fragile Bits [26]	0.2534	1.0923	0.2961	0.8284	0.0418	3.3054
BLPOC [29]	0.4022	0.4528	0.4396	0.2773	0.1136	2.6748
Log-Gabor [37]	0.2745	0.9266	0.2960	0.8280	0.0385	3.1525
This paper	**0.1196**	**2.5735**	**0.1986**	**1.8899**	**0.0290**	**6.4735**

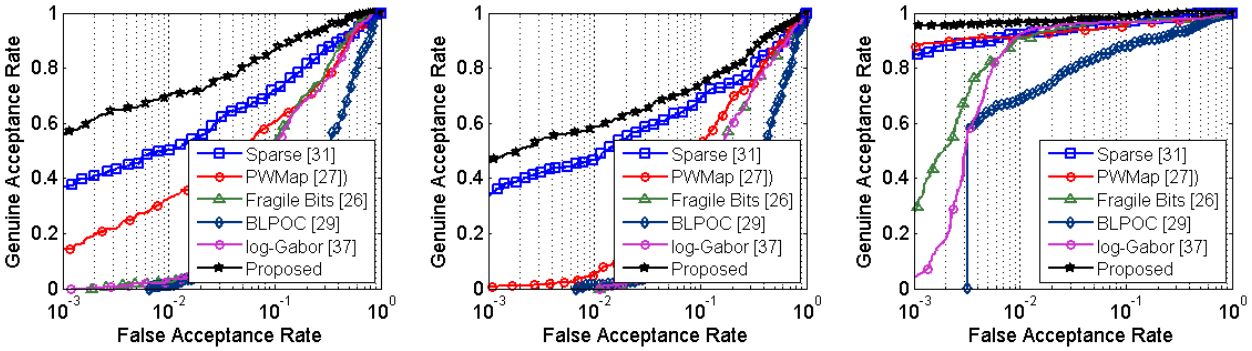

(a) (b) (c)

Fig. 9: Receiver operating characteristics from competing approaches on (a) UBIRIS.v2, (b) FRGC, (c) CASIA.v4-distance database.

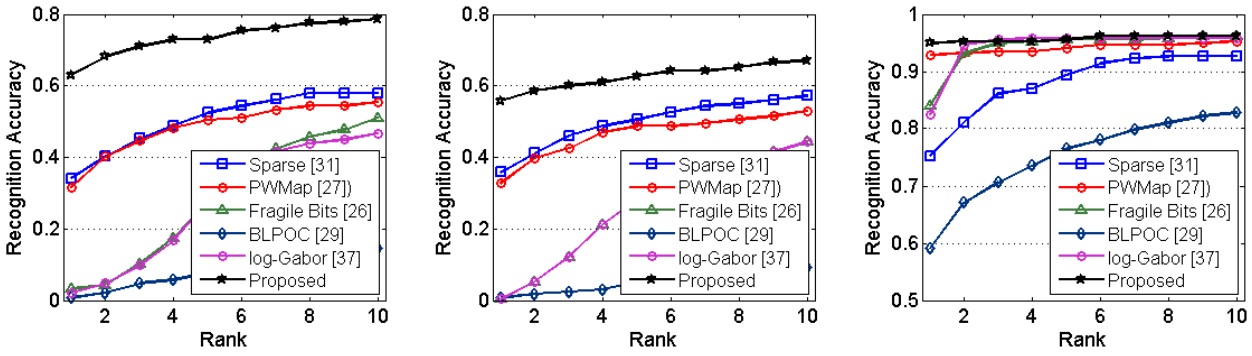

(a) (b) (c)

Fig. 10: Cumulative match curves from competing approaches on (a) UBIRIS.v2, (b) FRGC, (c) CASIA.v4-distance database.

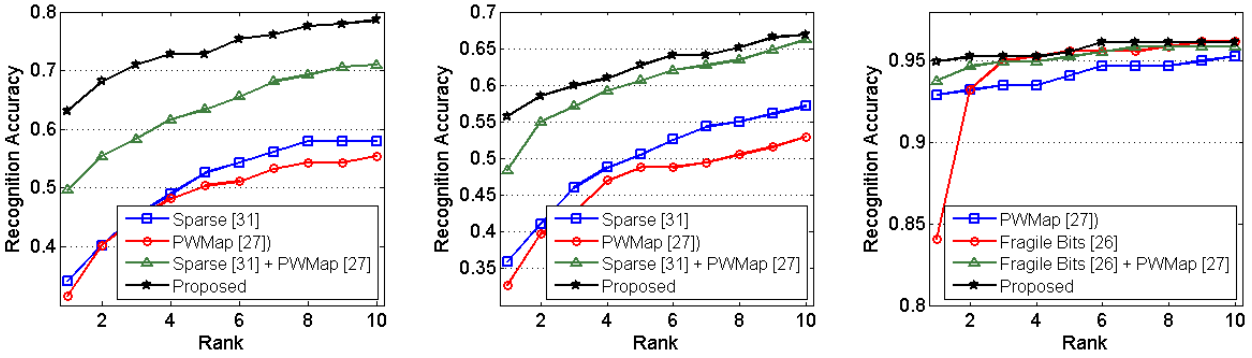

(a) (b) (c)

Fig. 11: Cumulative match curves from the comparison with the best two reported iris matching methods. (a) UBIRIS.v2, (b) FRGC, (c) CASIA.v4-distance database.

Table 5: Parameter employed for score combination.

Database	Methods	Weight		Rank-one Recognition Rate
		w_1	w_2	
UBIRIS.v2	1. PWMap [27] 2. Sparse [31]	0.49	0.51	49.6%
	Proposed: 1. Global 2. Local	0.43	0.57	**63%**
FRGC	1. PWMap [27] 2. Sparse [31]	0.49	0.51	48.4%
	Proposed: 1. Global 2. Local	0.485	0.515	**55.8%**
CASIA.v4-distance	1. PWMap [27] 2. Fragile Bits [26]	0.61	0.39	93.8%
	Proposed: 1. Global 2. Local	0.70	0.30	**95%**

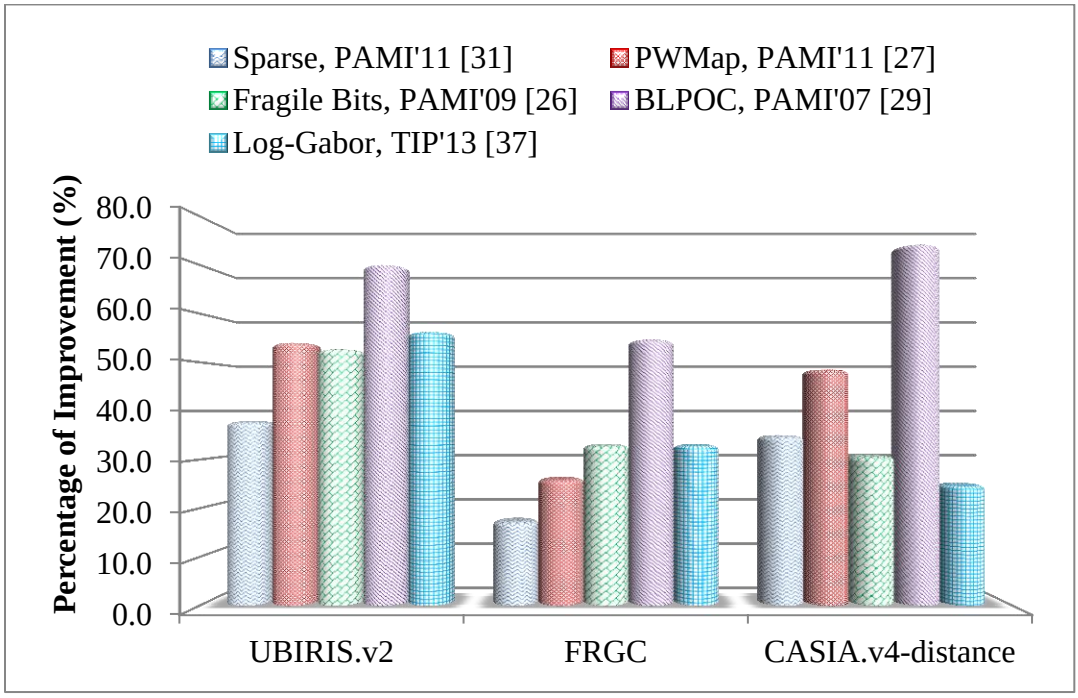

Fig. 12: Expected improvement in Equal Error Rate as compared to the competing approaches in literature.

6. Discussion

The recognition performance achieved by the proposed approach is quite encouraging, especially for the iris images acquired remotely using visible illumination and under less constrained environments. For example, the estimated decidability index of 2.5735 on UBIRIS.v2 database is comparable to the reported result from the winning algorithm ($d' = 2.5748$) in NICE.II competition [24], [32]. Such competition employed decidability index as the performance index in the evaluation of the iris matching algorithms participated in the competition. It is worth noting that the iris matching strategy investigated in this paper only employs the iris features and does not consider the multimodal (e.g. *periocular*) strategy as in the case of [32], which has been

declared as winning algorithm in the NICEII competition. Therefore, if we employ such combination strategy, the recognition performance improvement can also be expected. In order to validate such expectation, we provide the experimental result for the *joint* iris and periocular strategy on the UBIRIS.v2 database, as shown in Fig. 13. In this experiment, we employed dense SIFT [42], [43] as the feature descriptor for the segmented periocular region[**] and the matching scores were combined based weighted sum rule. The reported EER is observed to achieve the improvement from 0.1196 to 0.0435 while the decidability index is improved from 2.5735 to 3.5743 from using such joint strategy of iris and periocular features on the UBIRIS.v2. Therefore, the performance improvement by employing multimodal strategy, as in [32], is quite intuitive/expected. In addition, the participated algorithms in NICE.II competition were evaluated on the noise-free iris images[††], which may not be well-suited to provide accurate estimation of the actual performance for a deployable iris recognition system. As such, all the presented iris matching approaches in this paper were evaluated on the iris images which were segmented by employing a fully automated iris segmentation approach [37]. Therefore, our experimental results can better reflect the actual performance of *at-a-distance* iris recognition strategy acquired under *less constrained environments*.

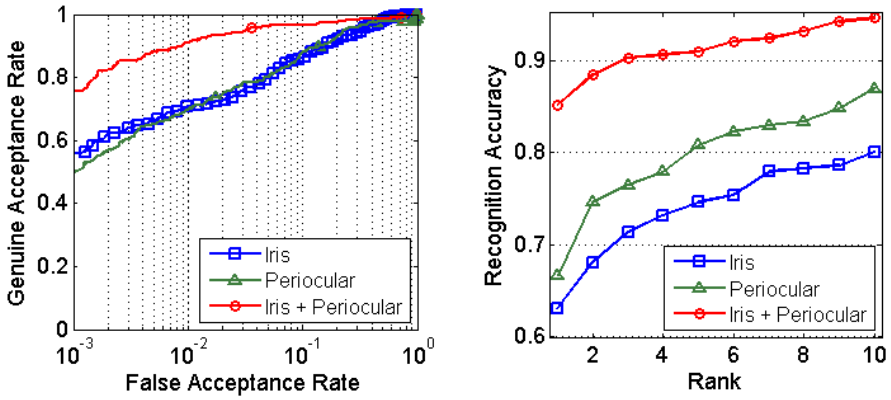

(a) (b)

Fig. 13: Recognition performance for the joint scores from iris and periocular features on UBIRIS.v2 database. (a) ROC, (b) CMC.

In spite of the superiority in the recognition performance as demonstrated from our experiments, the memory requirement and computational complexity are other important considerations should also be investigated. As such, we also analyze the memory requirements

[**] The periocular region is segmented using the approach as described in [37].
[††] The iris images are manually segmented and can be considered to have less influence (neglectable) from segmentation errors.

and the computational complexity of the proposed iris matching strategy based on the configurations as provided in Section 5.1. In order to provide the complexity analysis which can be independent across different implementation environments, we also employ the similar analysis approach as in [27] to investigate the complexity of the iris matching algorithm proposed in this paper. For the global iris feature representation, higher memory is required due to the remapping operation (Section 4.1). For example, the remapped dimension for a normalized iris image from the UBIRIS.v2 is 1024×128 bits (16 kB). The corresponding weight map requires 128 kB of the memory storage, such that the fraction values are quantized into the integers of range $[0,255]$ (1 byte). The memory storage required by the localized iris representation depends on a number of factors: (1) total number of image blocks, (2) order of ZMs, (3) repetition of ZMs, and (4) size of occlusion mask. The occlusion mask has the same dimensionality as the normalized iris image. For example, the dimension of occlusion mask for the UBIRIS.v2 is 512×64 bits (4 kilobytes). Due to the remapping operation in the global iris feature representation phase, the incurred computational cost in iris matching is expected to increase. For example, the global iris feature representation computed from the UBIRIS.v2 requires 2048 XOR operations on a 64-bit machine, 131072 element-wise weight multiplication operation (MUL) and a multiplication for the $1/\|W^j\|$ (can be precomputed during the weight map training phase). The incurred computational cost for the localized iris feature representation depends on the dimension of the computed feature vector. For instance, the dimension of the feature vector computed from a normalized iris image of the UBIRIS.v2 is $\mathbf{C}^{200}$ (complex number). The matching requires 200 element-wise multiplication operations, 200 element-wise division operations (DIV), 200 element-wise division operations to extract phase angles, and 200 multiplication (square) and incremental sum (INC) operations (approximation to the L2-norm). Table 6 summarizes the incurred memory storage and the computational cost as required by the proposed iris matching strategy on each of the employed databases. It is obvious to observe that higher computational cost is required for the global iris feature representation, which is mainly due to the employed block overlapping operation to account for spatial variations in the iris images acquired remotely under less constrained environments. In contrast, the localized iris feature representation requires much lower computational cost, which is mainly attributed to the low order moments of the computed ZMs features.

The choice of the ZMs parameters (n, m) were respectively obtained using the independent sets of training images from the three employed databases. The Zernike features with parameters (n, m) range from $(1, 1)$ to $(10, 10)$ are computed on the image blocks of various sizes. Fig. 14 shows such parameters estimation for the three employed databases. The choices of the parameters are quite consistent with several reported works [33], [34], [36], as higher-order moments are more sensitive to image noise. The decline in the recognition accuracy can be observed on the noisy datasets from the UBIRIS.v2 and FRGC databases when higher-order moments are employed in the computation of ZMs features but remain stable on the CASIA.v4-distance dataset (with relatively less influence from the noise on the NIR dataset).

Table 6: Memory requirement and the computational cost of the proposed iris matching strategy

Database	Memory Requirement per template (kilobyte)		Computational Cost (matching)	
	Global	*Localized*	*Global*	*Localized*
UBIRIS.v2	16 + 128	3.125 + 4	2048XOR + 131072MUL + 1MUL	200MUL + 200DIV + 200DIV + 200MUL + 200INC
FRGC	4 + 32	1.8125 + 1	512XOR + 32768MUL + 1MUL	116MUL + 116DIV + 116DIV + 116MUL + 116INC
CASIA.v4-distance	16 + 128	6.25 + 4	2048XOR + 131072MUL + 1MUL	400MUL + 400DIV + 400DIV + 400MUL + 400INC

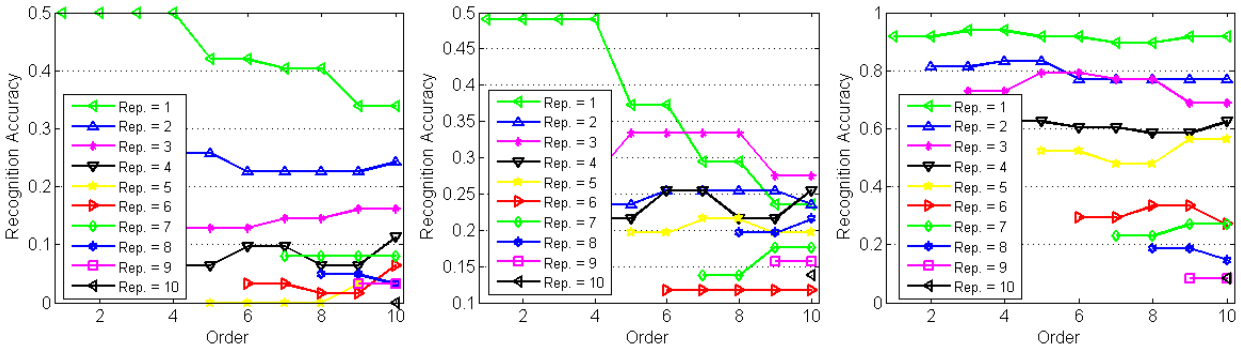

(a) (b) (c)

Fig. 14: Selection of the ZMs parameters for the database (a) UBIRIS.v2, (b) FRGC, (c) CASIA.v4-distance. Fig. (a)-(c) show only the parameters selection for the respective window size {25, 17, 25} employed in this paper due to the space limitation.

7. Conclusions

This paper has investigated a promising iris encoding and matching strategy for the iris images acquired at-a-distance, using both NIR and visible imaging, under less constrained environments. Such the images acquired at-a-distance and under less constrained imaging conditions are often degraded due to noise introduced by multiple sources, and therefore it is more likely to distort

the iris texture details (*e.g.* scale, rotation, blur, off-angle, occlusion, *etc*.). Therefore, the segmented iris images following the iris normalization step reveals the distorted texture details which can be varying even for the iris images from the same class. The joint strategy presented in this paper exploits a *global iris bits stabilization encoding strategy* and a *localized ZMs phase-based encoding strategy* to robustly recover the iris features. Our strategy has been to simultaneously ascertain the matching information from the local region pixels (which is more tolerant to the distortion) while also evaluating the matching information for the features which can preserve global matches from more stable texture patterns/regions. The global iris encoding is largely based on the recent promising effort on the fragile bits estimation [26]-[27]. The stability of the encoded iris features can be highly correlated with the consistency of the resulting iris bits, which can be estimated from the knowledge of the fragile bits. A nonlinear approach which can more effectively account for both consistencies of the iris bit and also for the overall quality of the weight map is employed to stabilize/weight the encoded iris bits. Therefore, the iris bits which are more likely to be corrupted by noise are penalized with lower weight values while the consistent bits are rewarded with higher values. In this paper, we also proposed a new approach to encode iris features by recovering ZM phase correlation in localized iris regions. ZMs have been known to constitute good image features which are robust to image variations and multiple noise sources which are commonly observed in the at-a-distance iris images acquired under less constrained environments. The iris features encoded using ZM phase descriptors are computed from the partially overlapping blocks extracted from the normalized iris image. A joint strategy to simultaneously employ the encoded global and localized iris features can benefit from both of these approaches. The reported experimental results by the proposed iris encoding and matching strategy on three publicly available databases: UBIRIS.v2, FRGC, CASIA.v4-distance have shown to be promising, which achieve the average improvements of *54.3%, 32.7%* and *42.6%* in EER, respectively, as compared to several competing iris matching algorithms. Despite the encouraging results obtained by the proposed iris matching strategy, further efforts are required to improve the matching accuracy, especially for the visible-light iris matching in order to make any inroads to the commercial applications. Efficiency of the iris matching algorithm and the recognition accuracy are the two prime criterions for selecting an algorithm for the deployment. Therefore, further efforts should also be

directed to develop more efficient iris matching algorithms which can simultaneously operate on images acquired in dynamic spectral illumination under less constrained environments.

Acknowledgment

We gracefully acknowledge the SOCIA Lab (University of Beira Interior, Portugal), NIST (USA) and Institute of Automation (Chinese Academy of Sciences, China) for their contributions of the databases employed in this work. This work is partially supported by the PolyU project G-YK78.

References

[1] K. Bowyer, K. Hollingsworth and P. Flynn, "Image understanding for iris biometrics: A survey," *Image Vision Comput.,* vol. 110, no. 2, pp. 181-307, 2008.

[2] J. Daugman, "How iris recognition works," *IEEE Trans. Circuits Syst. Video Technol.,* vol. 14, no. 1, pp. 21-30, 2004.

[3] J. Daugman, "New methods in iris recognition,," *IEEE Trans. Syst. Man Cybern. Part B Cybern.,* vol. 37, no. 5, p. 1167–1175, 2007.

[4] R. Wildes, "Iris Recognition: An emerging biometric technology," *Proc. IEEE,* vol. 85, no. 9, pp. 1348-1363, 1997.

[5] Z. He, T. Tan, Z. Sun and X. Qiu, “Toward accurate and fast iris segmentation for iris biometrics,” *IEEE Trans. Pattern Anal. Mach. Intell.,* vol. 31, no. 9, p. 1670–1684, 2009.

[6] Y. Zhou and A. Kumar, "Personal identification from iris images using localized Radon transform," *Proc. ICPR 2010,* pp. 2840 – 2843, Istanbul, Aug. 2010.

[7] A. Kumar and A. Passi, “Comparison and combination of iris matchers for reliable personal authentication,” *Pattern Recognit.,* vol. 43, no. 3, p. 1016–1026, 2010.

[8] "Role of biometric technology in Aadhaar enrollments, UID Authority of India," Jan 2012. [Online]. Available: http://uidai.gov.in/images/FrontPageUpdates/role_of_biometric_technology_in_aadhaar_jan21_2012.pdf.

[9] K. Bowyer, "The results of the NICE.II iris biometrics competition," *Pattern Recognit. Lett.,* vol. 33, no. 8, pp. 965-969, 2012.

[10] J. Matey, O. Naroditsky, K. Hanna, R. Kolczynski, D. LoIacono, S. Mangru, M. Tinker, T. Zappia and W. Zhao, "Iris on the move: acquisition of images for iris recognition in less constrained environments,," *Proc. IEEE,* vol. 94, no. 11, pp. 1936-1947, 2006.

[11] S. Venugopalan, U. Prasad, K. Harun, K. Neblett, D. Toomey, J. Heyman and M. Savvides, "Long range iris acquisition system for stationary and mobile subjects," *Proc. IJCB 2011,* p. 1–8, 2011.

[12] H. Proenca and L. Alexandre, "UBIRIS: A noisy iris image database," *Proc. ICIAP 2005, Intern. Conf. Image Analysis and Processing,* 2005.

[13] H. Proenca, S. Filipe, R. Santos, J. Oliveira and L. Alexandre, "The UBIRIS.v2: A database of visible wavelength images captured on the move and at-a-distance," *IEEE Trans. Pattern Anal. Mach. Intell.,* vol. 32, no. 8, pp. 1529-1535, 2010.

[14] H. Proenca, "Iris recognition: on the segmentation of degraded images acquired in the visible wavelength," *IEEE Trans. Pattern Anal. Mach. Intell.,* vol. 32, no. 8, pp. 1502-1516, 2010.

[15] C.-W. Tan and A. Kumar, "Automated segmentation of iris images using visible wavelength face images," *Proc. CVPR 2011, Colorado Springs,* pp. 9-14, 2011.

[16] C.-W. Tan and A. Kumar, "A unified framework for automated iris segmentation using distantly acquired face images," *IEEE Trans. Image Process.,* vol. 21, no. 9, pp. 4068-4079, 2012.

[17] T. Tan, Z. He and Z. Sun, "Efficient and robust segmentation of noisy iris images for non-cooperative iris recognition," *Image Vision Comput.,* vol. 28, no. 2, pp. 223-230, 2010.

[18] D. S. Jeong, J. W. Hwang, B. J. Kang, K. R. Park, C. S. Won, D.-K. Park and J. Kim, "A new iris segmentation method for

non-ideal iris images," *Image Vision Comput.,* vol. 28, no. 2, pp. 254-260, 2010.

[19] A. Kumar, T.-S. Chan, "Iris recognition using quaternionic sparse orientation code (QSOC)," *Proc. CVPR 2012,* Providence, pp. 1-6, CVPRW'12, Jun. 2012.

[20] W. Sankowski, K. Grabowski, M. Napieralska, M. Zubert and A. Napieralski, "Reliable algorithm for iris segmentation in eye image," *Image Vision Comput.,* vol. 28, no. 2, pp. 231-237, 2010.

[21] R. D. Labati and F. Scotti, "Noisy iris segmentation with boundary regularization and reflections removal,," *Image Vision Comput.,* vol. 28, no. 2, p. 270–277, 2010.

[22] Y. Chen, M. Adjouadi, C. Han, J. Wang, A. Barreto, N. Rishe and J. Andrian, "A highly accurate and computationally efficient approach for unconstrained iris segmentation,," *Image Vision Comput.,* vol. 28, no. 2, p. 261–269, 2010.

[23] M. A. Luengo-Oroz, E. Faure and J. Angulo, "Robust iris segmentation on uncalibrated noisy images using mathematical morphology,," *Image Vision Comput.,* vol. 28, no. 2, p. 278–284, 2010.

[24] "NICE:II - Noisy Iris Challenge Evaluation, Part II.," [Online]. Available: http://nice2.di.ubi.pt/.

[25] H. Proenca and L. Alexandre, "Toward covert iris biometric recognition: experimental results from the NICE contests," *IEEE Trans. Inf. Forensics Secur.,* vol. 7, pp. 798-808, 2012.

[26] K. Hollingsworth, K. Bowyer and P.J. Flynn, "The best bits in an iris code," *IEEE Trans. Pattern Anal. Mach. Intell.,* vol. 31, no. 6, pp. 964-973, 2009.

[27] D. Wenbo, S. Zhenan and T. Tieniu, "Iris matching based on personalized weight map," *IEEE Trans. Pattern Anal. Mach. Intell,* vol. 33, no. 9, pp. 1744-1757, 2011.

[28] D. Monro, S. Rakshit and D. Zhang, "DCT-based iris recognition," *IEEE Trans. Pattern Anal. Mach. Intell.,* vol. 29, no. 4, pp. 586-595, 2007.

[29] K. Miyazawa, K. Ito, T. Aoki, K. Kobayashi and H. Nakajima, "An effective approach for iris recognition using phase-based image matching,," *IEEE Trans. Pattern Anal. Mach. Intell.,* vol. 30, p. 1741–1756, 2007.

[30] Z. Sun and T. Tan, "Ordinal measures for iris recognition," *IEEE Trans. Pattern Anal. Mach. Intell.,* vol. 31, no. 12, pp. 2211-2226, 2009.

[31] J. Pillai, V. Patel, R. Chellappa and N. Ratha, "Secure and robust iris recognition using random projections and sparse representations," *IEEE Trans. Pattern Anal. Mach. Intell,* vol. 33, pp. 1877-1893, 2011.

[32] T. Tan, X. Zhang, Z. Sun and H. Zhang, "Noisy iris image matching by using multiple cues," *Pattern Recognit. Lett.,* vol. 33, no. 8, pp. 979-977, 2012.

[33] A. Khotanzad and Y. H. Hong, "Invariant image recognition by Zernike moments," *IEEE Trans. Pattern Anal. Mach. Intell.,* vol. 12, no. 5, pp. 489-497, 1990.

[34] C.-H. Teh and R. Chin, "On image analysis by the methods of moments," *IEEE Trans. Pattern Anal. Mach. Intell.,* vol. 10, no. 4, pp. 496-513, 1998.

[35] J. Revaud, G. Lavoue and A. Baskurt, "Improving Zernike moments comparison for optimal similarity and rotation angle retrieval," *IEEE Trans. Pattern Anal. Mach. Intell.,* vol. 31, no. 4, pp. 627-636, 2009.

[36] Z. Chen and S.-K. Sun, "A Zernike moment phase-based descriptor for local image representation and matching," *IEEE Trans. Image Process.,* vol. 19, no. 1, pp. 205-219, 2010.

[37] C.-W. Tan and A. Kumar, "Towards online iris and periocular recognition under relaxed imaging constraints," *IEEE Trans. Image Process.,* vol. 22, no. 10, pp. 3751-3765, 2013.

[38] "Face Recognition Grand Challenge – Overview.," [Online]. Available: http://www.nist.gov/itl/iad/ig/frgc.cfm.

[39] P. Phillips, P. Flynn, T. Scruggs, K. Bowyer, J. Chang, K. Hoffman, J. Marques, J. Min and W.Worek, "Overview of the face recognition grand challenge," *Proc. CVPR 2005,* 2005.

[40] "CASIA.v4 Database.," [Online]. Available: http://biometrics.idealtest.org/dbDetailForUser.do?id=4.

[41] L. Masek and P. Kovesi, "MATLAB source code for a biometric identification system based on iris patterns," The School of Computer Science and Software Engineering, The University of Western Australia, 2003. [Online]. Available: http://www.csse.uwa.edu.au/~pk/studentprojects/libor/.

[42] D. G. Lowe, "Distinctive image features from scale-invariant keypoints," *International Journal of Computer Vision*,vol. 60, no. 2, pp. 91–110, 2004.

[43] VLFeat: An open and portable library of computer vision algorithms. http://www.vlfeat.org/.

[44] J. Daugman, "Iris recognition at airports and border crossings," pp. 819-825, in *Encyclopedia of Biometrics*, S. Z. Li and A. K. Jain (*Eds*), Springer, 2009.

[45] C.W. Tan and Ajay Kumar, "Adaptive and localized iris weight map for accurate iris recognition under less constrained environments," *IEEE Int'l Conf. Biometrics Theory and Applications,* BTAS, 2013

[46] C. Boyce, A. Ross, M. Monaco, L. Hornak and L. Xin, "Multispectral iris analysis: A preliminary study," *Proc. CVPRW 2006*, pp.51-51, 2006.

[47] J. Reyes-Lopez, S. Campos, H. Allende and R. Salas, "Zernike's feature descriptors for iris recognition with SVM," *Proc. of Int' Conf. of the Chilean Computer Science Society*, pp.283-288, 2011.

[48] OpenCV. http://opencv.org/.